

Mapping the Hubble Flow from $z \sim 0$ to $z \sim 7.5$ with HII Galaxies

R. Chávez^{1,2*}, R. Terlevich^{3,4,5}, E. Terlevich^{3,4,5}, A. L. González-Morán^{3,6}, D. Fernández-Arenas^{7,1,3}, F. Bresolin⁸, M. Plionis^{9,10,11}, S. Basilakos^{12,13,14}, R. Amorín¹⁵ and M. Llerena¹⁶

¹Universidad Nacional Autónoma de México, Instituto de Radioastronomía y Astrofísica, 58090, Morelia, Michoacán, México

²Secretaría de Ciencia, Humanidades, Tecnología e Innovación, Av. Insurgentes Sur 1582, 03940, Ciudad de México, México

³Instituto Nacional de Astrofísica, Óptica y Electrónica, Tonantzintla, Puebla, México

⁴Institute of Astronomy, University of Cambridge, Cambridge, CB3 0HA, UK

⁵Facultad de Astronomía y Geofísica, Universidad de La Plata, La Plata, Argentina

⁶Universidad Pedagógica del Estado de Sinaloa, Culiacán, Sinaloa, 80027, México

⁷Canada–France–Hawaii Telescope, Kamuela, 96743 HI, USA

⁸Institute for Astronomy, University of Hawaii, 2680 Woodlawn Drive, 96822 Honolulu, HI USA

⁹National Observatory of Athens, Lofos Nymfon, 11852 Athens, Greece

¹⁰Physics Dept., Aristotle Univ. of Thessaloniki, Thessaloniki 54124, Greece

¹¹CERIDES, Center of Excellence in Risk & Decision Sciences, European University of Cyprus, Cyprus

¹²National Observatory of Athens, P. Pendeli, Athens, Greece

¹³Academy of Athens, Research Center for Astronomy and Applied Mathematics, Soranou Efessiou 4, 11527, Athens, Greece

¹⁴School of Sciences, European University Cyprus, Diogenes Street, Engomi, 1516 Nicosia, Cyprus

¹⁵Instituto de Astrofísica de Andalucía (CSIC), Apartado 3004, 18080 Granada, Spain

¹⁶INAF - Osservatorio Astronomico di Roma, Via di Frascati 33, 00078, Monte Porzio Catone, Italy

MN-24-2288-MJ.R1 — Compiled at 1:12 hrs on 4 March 2025

ABSTRACT

Over twenty years ago, Type Ia Supernovae (SNIa) observations revealed an accelerating Universe expansion, suggesting a significant dark energy presence, often modelled as a cosmological constant, Λ . Despite its pivotal role in cosmology, the standard Λ CDM model remains largely underexplored in the redshift range between distant SNIa and the Cosmic Microwave Background (CMB). This study harnesses the James Webb Space Telescope’s advanced capabilities to extend the Hubble flow mapping across an unprecedented redshift range, from $z \approx 0$ to $z \approx 7.5$. Using a dataset of 231 HII galaxies and extragalactic HII regions, we employ the $L - \sigma$ relation that correlates the luminosity of Balmer lines with their velocity dispersion, to define a competitive technique for measuring cosmic distances. This approach allows the mapping of the Universe expansion history over more than 12 billion years, covering 95% of its age. Our analysis, using Bayesian inference, constrains the parameter space $\{h, \Omega_m, w_0\} = \{0.731 \pm 0.039, 0.302_{-0.069}^{+0.12}, -1.01_{-0.29}^{+0.52}\}$ (statistical) for a flat Universe. Our results provide new insights into cosmic evolution and imply a lack of change in the photo-kinematical properties of the young massive ionizing clusters in HII galaxies across most of the history of the Universe.

Key words: galaxies: starburst – dark energy – cosmology: parameters

1 INTRODUCTION

The first conclusive evidence supporting the accelerated expansion of the Universe was presented over two decades ago through the analysis of Type Ia Supernovae (SNIa) data (Riess et al. 1998; Perlmutter et al. 1999). Subsequent studies involving cosmic microwave background (CMB) anisotropies (e.g. Jaffe et al. 2001; Pryke et al. 2002; Spergel et al. 2007; Planck Collaboration et al. 2014, 2016) and Baryon Acoustic Oscillations (BAOs) (e.g. Eisenstein et al. 2005; Blake et al.

2011), along with independent measurements of the Hubble parameter (e.g. Chávez et al. 2012; Freedman et al. 2012; Riess et al. 2016, 2018; Fernández Arenas et al. 2018), have robustly confirmed the existence of a dark energy (DE) component in the Universe.

Observational campaigns targeting high redshift (z) cosmological tracers are underway to refine our understanding of the DE Equation of State (EoS). A central objective is to ascertain if the w parameter, which determines the relationship between pressure p and the mass-energy density ρc^2 within the DE EoS, undergoes evolution over cosmic time (Peebles & Ratra 1988; Wetterich 1988). By rigorously constraining cosmological parameters and cross-validating findings via di-

* E-mail: r.chavez@irya.unam.mx

verse, independent methodologies, we aim to produce a more accurate and resilient cosmological framework.

H II galaxies (HIIGs) represent intense and compact star formation episodes predominantly found in dwarf irregular galaxies, where they significantly contribute to the overall luminosity. HIIGs are spectroscopically selected as the star forming systems with the largest equivalent width of their Balmer emission lines ($EW(H\beta) > 50 \text{ \AA}$). This selection criterion guarantees that HIIGs are the youngest systems ($\lesssim 5 \text{ Myr}$) that can be studied in detail. Similarly, giant extragalactic H II regions (GEHRs) are associated with vigorous star formation, but they are typically situated in the outer disks of late-type galaxies. Notably, the rest-frame optical spectra of both GEHRs and HIIGs are virtually indistinguishable from each other, marked by pronounced emission lines. These lines arise from gas ionisation events triggered by a massive Young Stellar Cluster (YSC) or an ensemble of such clusters, often referred to as a Super Star Cluster (SSC) (Searle & Sargent 1972; Bergeron 1977; Terlevich & Melnick 1981; Kunth & Östlin 2000; Chávez et al. 2014).

The pronounced emission lines in the rest-frame optical spectra of GEHRs and HIIGs position them as potent probes for investigating young star formation at high- z . With instruments such as NIRSpec (Dorner, B. et al. 2016) onboard the JWST (Gardner et al. 2006), it becomes feasible to delve into these regions up to $z \sim 6.5$ via the $H\alpha$ emission line or even up to $z \sim 9$ using the $H\beta$ and [OIII] $\lambda\lambda 4959, 5007 \text{ \AA}$ emission lines. Consequently, this allows for the observation of luminous HIIGs, tracing back to and including the epoch of reionisation.

Multiple studies have proven that both HIIGs and GEHRs exhibit a correlation between their Balmer lines luminosity, e.g. $L(H\beta)$, and the ionised gas velocity dispersion, σ , traced by these emission lines. This correlation, known as the $L - \sigma$ relation (Terlevich & Melnick 1981; Melnick et al. 1988; Bordalo & Telles 2011; Chávez et al. 2014), serves as a powerful cosmological distance indicator (Plionis et al. 2011; Chávez et al. 2016; González-Morán et al. 2019, 2021), where GEHRs and nearby HIIGs are used as the ‘‘anchor’’ sample because their distances can be independently estimated from Cepheid variables or Tip of the Red Giant Branch (TRGB) measurements (Chávez et al. 2012; Fernández Arenas et al. 2018). Consequently, the $L - \sigma$ relation offers a unique avenue for employing this distance estimator to study the Hubble flow across a vast z range.

In this work we present the use of the $L - \sigma$ relation of GEHRs and HIIGs as a cosmological tracer up to $z \sim 7.5$ and the resulting constraints to cosmological parameters. Our analysis demonstrates the efficacy of GEHRs and HIIGs in tracing the evolution of the Universe, offering insights into the dynamics of the cosmic expansion and the distribution of matter across a significant fraction of cosmic history. The results presented herein covering an unprecedented redshift range, from 0.0 to ~ 7.5 , contribute to the ongoing efforts to constrain cosmological models with greater precision, utilising the unique properties of these astrophysical objects.

2 DATA SETS

The dataset employed in this study is derived from a comprehensive compilation sourced from multiple previously published works:

- The anchor sample of 36 nearby objects with independently measured distance moduli was presented and studied in Fernández Arenas et al. (2018) and references therein.
- At low z ($0.01 \leq z \leq 0.15$), we use 107 HIIGs extensively analysed in Chávez et al. (2014).
- At intermediate z ($0.6 \leq z \leq 4$) we included 24 HIIGs from Erb et al. (2006), Masters et al. (2014) and Maseda et al. (2014), our 6 HIIGs observed with VLT-XShooter published in Terlevich et al. (2015), 15 HIIGs observed with Keck-MOSFIRE and presented in González-Morán et al. (2019) and 29 HIIGs observed with VLT-KMOS and presented in González-Morán et al. (2021). Here we also include 9 new HIIGs first presented in Llerena et al. (2023).
- At high z ($4 \leq z \leq 7.5$) we include 5 new HIIGs observed with JWST-NIRSpec as part of the JWST Advanced Deep Extragalactic Survey (JADES) (Bunker et al. 2024) and first presented in de Graaff et al. (2024).

The newly collected data for HIIGs, which extends our previously published data is given in Table 1. This dataset integrates the 5 HIIGs observed through JWST-NIRSpec, as described in de Graaff et al. (2024), along with 9 HIIGs from Llerena et al. (2023). Recognising the well-documented disparity in velocity dispersion measurements (σ) measured either with the [OIII] or the Balmer lines, a correction of 2.1 km s^{-1} (Chávez et al. 2016) derived from data with both measurements, was applied to three JWST-NIRSpec HIIGs which do not have σ measured from Balmer emission lines. Additionally, we performed extinction corrections on all the $H\beta$ flux measurements, following the extinction law in Gordon et al. (2003). The Balmer decrement, derived from $H\alpha$ and $H\beta$ fluxes, was primarily used in the JWST-NIRSpec data and most of the VUDS/VANDELS dataset (Llerena et al. 2023) for extinction correction. Where $H\alpha$ fluxes were not available, we applied the mean extinction value from the VUDS/VANDELS data.

3 CONSTRAINTS ON COSMOLOGICAL PARAMETERS

To rigorously define the cosmological parameters within the scope of this study, we employ a refined methodology, building upon the foundational approach delineated in our preceding works (Chávez et al. 2016; González-Morán et al. 2019). A succinct overview of this methodology is presented below to facilitate a comprehensive understanding.

The likelihood function used for the analysis of GEHRs and HIIGs is expressed as:

$$\mathcal{L}_H \propto \exp\left(-\frac{1}{2}\chi_H^2\right), \quad (1)$$

where the chi-squared (χ_H^2) term is defined by:

$$\chi_H^2 = \sum_n \frac{(\mu_o(\log f, \log \sigma | \alpha, \beta) - \mu_\theta(z|\theta))^2}{\epsilon^2}. \quad (2)$$

Here μ_o represents the ‘observed’ distance modulus, derived

Table 1. Data set measurements used in the analysis.

Object	z	$\log \sigma$ (km s ⁻¹)	$\log f(\text{H}\beta)$ (erg s ⁻¹ cm ⁻²)	$EW(\text{H}\beta)$ (Å)
JWST data				
JADES-NS-00016745	5.56616 ± 0.00011 ^a	1.731 ± 0.016 ^b	-17.64 ± 0.21 ^d	135.35 ± 10.47 ^f
JADES-NS-10016374	5.50411 ± 0.00007 ^a	1.785 ± 0.014 ^b	-18.14 ± 0.20 ^d	212.74 ± 12.53 ^f
JADES-NS-00019606	5.88979 ± 0.00008 ^a	1.622 ± 0.019 ^c	-18.11 ± 0.27 ^d	242.15 ± 48.25 ^f
JADES-NS-00022251	5.79912 ± 0.00007 ^a	1.621 ± 0.011 ^c	-17.86 ± 0.11 ^d	208.52 ± 9.64 ^f
JADES-NS-00047100	7.43173 ± 0.00015 ^a	1.868 ± 0.024 ^c	-17.62 ± 0.39 ^e	
VUDS data				
5101421970	2.4710 ± 0.00025 ^g	1.706 ± 0.022 ^g	-16.35 ± 0.14 ^h	49.72 ± 3.01 ^h
510996058	2.4935 ± 0.00025 ^g	1.740 ± 0.094 ^g	-16.62 ± 0.42 ^h	50.55 ± 13.64 ^h
511001501	2.2247 ± 0.00022 ^g	1.779 ± 0.028 ^g	-16.05 ± 0.08 ^h	197.56 ± 10.72 ^h
5101444192	3.4205 ± 0.00034 ^g	1.845 ± 0.017 ^g	-16.31 ± 0.16 ^h	144.67 ± 25.55 ^h
VANDELS data				
UDS022487	3.0679 ± 0.00031 ^g	1.710 ± 0.031 ^g	-16.55 ± 0.15 ^h	85.33 ± 8.95 ^h
CDFS020954	3.4993 ± 0.00035 ^g	1.761 ± 0.085 ^g	-16.42 ± 0.14 ^h	152.87 ± 8.2 ^h
CDFS022799	2.5457 ± 0.00025 ^g	1.787 ± 0.017 ^g	-16.31 ± 0.07 ^h	80.3 ± 3.83 ^h
UDS020394	3.3076 ± 0.00033 ^g	1.842 ± 0.014 ^g	-16.72 ± 0.15 ^h	125.37 ± 19.01 ^h
CDFS018182	2.3174 ± 0.00023 ^g	1.850 ± 0.016 ^g	-16.37 ± 0.08 ^h	50.43 ± 2.57 ^h

^aTaken from de Graaff et al. (2024). ^bMeasured from the H α line in de Graaff et al. (2024) and corrected by thermal broadening. ^cMeasured from the [OIII] line in de Graaff et al. (2024) and corrected by thermal broadening then corrected to the Balmer lines value (see the text). ^dTaken directly from the JADES DR2 catalogue (Bunker et al. 2024) and corrected by extinction (see the text). ^eObtained from Baker et al. (2025) and corrected for extinction. ^fMeasured directly from JADES spectra. ^gM. Llerena, personal communication. ^hTaken from Llerena et al. (2023).

from the observables via the $L - \sigma$ relation,

$$\mu_o = 2.5(\beta \log \sigma + \alpha - \log f - 40.08), \quad (3)$$

where α and β are respectively the $L - \sigma$ relation's intercept and slope, $\log \sigma$ is the logarithm of the velocity dispersion, corrected for broadening (thermal and instrumental), and $\log f$ is the logarithm of the extinction corrected flux. In the other hand μ_θ denotes, for HIIGs, the distance modulus derived from a cosmological model with parameters θ and the measured redshift z , while for our anchor sample it represents the distance modulus measured via a primary distance indicator.

In Equation 2, the theoretical distance modulus, μ_θ , is a function of a set of cosmological parameters. In the broadest scenario considered in this study, these parameters are denoted as $\theta = \{h, \Omega_m, w_0, w_a\}$, in addition to the redshift, z . The parameters w_0 and w_a are pivotal in defining the DE EoS. Its general form is given by:

$$p_w = w(z)\rho_w c^2, \quad (4)$$

where p_w represents the pressure, and ρ_w denotes the density of DE. The function $w(z)$ characterises the evolving DE EoS parameter. Various DE models have been proposed and explored, many of which employ a Taylor expansion around the present epoch. A notable example is the Chevallier-Polarski-Linder (CPL) parametrization (Chevallier & Polarski 2001; Linder 2003; Peebles & Ratra 2003; Dicus & Repko 2004; Wang & Mukherjee 2006), which is expressed as:

$$w(z) = w_0 + w_a \frac{z}{1+z}. \quad (5)$$

The cosmological constant, denoted as Λ , is just a special case of DE, given for $(w_0, w_a) = (-1, 0)$ while the so called

wCDM models are such that $w_a = 0$ but w_0 can take values $\neq -1$.

In the likelihood function, the weights are quantified by ϵ^2 , which encapsulates various sources of uncertainties. This is formally represented as:

$$\epsilon^2 = \epsilon_{\mu_o, \text{stat}}^2 + \epsilon_{\mu_\theta, \text{stat}}^2 + \epsilon_{\text{sys}}^2, \quad (6)$$

where $\epsilon_{\mu_o, \text{stat}}$ denotes the statistical uncertainties of the observed distance modulus, defined by:

$$\epsilon_{\mu_o, \text{stat}}^2 = 6.25 (\epsilon_{\log f}^2 + \beta^2 \epsilon_{\log \sigma}^2 + \epsilon_\beta^2 \log \sigma^2 + \epsilon_\alpha^2). \quad (7)$$

Here, $\epsilon_{\log f}$, $\epsilon_{\log \sigma}$, ϵ_α , and ϵ_β represent the uncertainties associated with the logarithm of the flux, the logarithm of the velocity dispersion, and the intercept and slope of the $L - \sigma$ relation, respectively. Furthermore, $\epsilon_{\mu_\theta, \text{stat}}$ in Equation 6 refers to the statistical uncertainty associated with the theoretical distance modulus. This uncertainty originates from the redshift uncertainty in the case of HIIGs, and from the primary distance indicator measurement uncertainty for the anchor sample. Lastly, ϵ_{sys} encompasses the systematic uncertainties.

In the pursuit of a more versatile analysis framework, we have also established an h -free likelihood function, as suggested by Nesseris & Perivolaropoulos (2005). This involves a rescaling of the luminosity distance (d_L) through the introduction of a dimensionless luminosity distance, $D_L(z, \theta)$, defined as:

$$D_L(z, \theta) = (1+z) \int_0^z \frac{dz'}{E(z', \theta)} \quad (8)$$

In this formulation, d_L is expressed as $d_L = cD_L/H_0$. This rescaling technique is employed to ascertain cosmological parameters independently of the Hubble constant, a method-

ology comprehensively detailed in [González-Morán et al. \(2019\)](#). Here $E(z, \theta)$ for a flat Universe is given by:

$$E^2(z, \theta) = \Omega_r(1+z)^4 + \Omega_m(1+z)^3 + \Omega_w(1+z)^{3y} \exp\left(\frac{-3w_a z}{1+z}\right) \quad (9)$$

with $y = (1 + w_0 + w_a)$ and Ω_r the radiation density parameter, such that we can define $\Omega_w = 1 - \Omega_m - \Omega_r$.

In our analysis, we employ the MultiNest Bayesian inference algorithm ([Feroz & Hobson 2008](#); [Feroz et al. 2009, 2019](#)) to optimise the likelihood function, thereby deriving constraints on various combinations of nuisance and cosmological parameters. Uniform uninformative priors are consistently used in all cases (cf. [González-Morán et al. 2021](#)).

In order to facilitate a comprehensive comparison of our derived constraints with existing studies, we have adopted the figure of merit (FoM) as defined by [Wang \(2008\)](#). This FoM is quantitatively expressed as:

$$FoM = \frac{1}{\sqrt{\det \text{Cov}(\theta_0, \theta_1, \theta_2, \dots)}} \quad (10)$$

where, $\text{Cov}(\theta_0, \theta_1, \theta_2, \dots)$ represents the covariance matrix corresponding to the parameter set $\{\theta_i\}$. This metric provides a robust quantitative basis for evaluating and comparing the precision of different cosmological parameter estimations.

4 RESULTS

Using our compiled dataset of 231 objects from our HIIGs and anchor samples, we have derived constraints applicable to various cosmological models. The derived constraints on various cosmological and nuisance parameters are detailed in [Table 2](#). This table presents the marginalised best-fit values alongside their corresponding 1σ uncertainties for each parameter. Note that parameters enclosed in parentheses were held constant during the analysis, in this cases we adopted their values as in [González-Morán et al. \(2021\)](#). Also, the table encompasses combined analyses of both HIIGs and our anchor samples, as well as scenarios where only the HIIGs sample is employed.

Our main focus consists on constraining a generalised parameter space, denoted as $\theta = \{\alpha, \beta, h, \Omega_m, w_0, w_a\}$. Here, $\theta_n = \{\alpha, \beta\}$ represents nuisance parameters, specifically characterising the $L - \sigma$ relation for GEHRs and HIIGs, where α is the intercept and β the slope of this relation. The remainder of the parameter space pertains to distinct cosmological models. For the flat Λ CDM model, the parameters are defined as $\theta_c = \{h, \Omega_m, -1, 0\}$, indicating that we constrain the reduced Hubble constant $h = H_0/(100 \text{ km s}^{-1} \text{ Mpc}^{-1})$ and the total matter density parameter, Ω_m , while maintaining constant the first two DE EoS parameters at $w_0 = -1$ and $w_a = 0$. This specific setting aligns with a cosmological constant (Λ). Extending the constraints to include the value of w_0 allows for an evolving DE EoS, characteristic of models akin to quintessence ([Ratra & Peebles 1988](#); [Wetterich 1988](#)). Lastly, incorporating a constraint on w_a aligns with the Chevallier-Polarski-Linder (CPL) model, as delineated in the seminal works ([Chevallier & Polarski 2001](#); [Linder 2003](#); [Peebles & Ratra 2003](#)).

In the first two rows of [Table 2](#) we use our h free approach, so α and h are not present in the analysis and we fix the value of β as discussed above, so we do not employ the anchor

sample data. In the following two rows of the table, we include constraints on h but fix the values of the nuisance parameters, α and β , so again we do not employ the anchor sample. In the last four rows of the table, we show the results including the anchor sample, so that we are constraining simultaneously nuisance and cosmological parameters. The fact that in all cases the values of the nuisance parameters, α and β , are consistent at the level 1σ shows the stability of the analysis and the constraints on the $L - \sigma$ relation.

In [Figure 1](#) we present the Hubble diagram for the HIIGs and anchor samples. In magenta we plot the anchor sample of 36 objects which have been analysed in [Fernández Arenas et al. \(2018\)](#), in blue we present the full sample of 181 HIIGs from [González-Morán et al. \(2021\)](#), while in red we show the 9 new HIIGs from [Llerena et al. \(2023\)](#) and in green 5 HIIGs newly observed with JWST from [de Graaff et al. \(2024\)](#). The black line is the cosmological model that best fits the data with the red shaded area representing the 1σ uncertainties to the model, while the grey dashed line is a flat cosmological model without dark energy. The inset at the left shows a close-up of the Hubble diagram for $z \leq 0.15$. The inset at the right presents the normalised residuals (or ‘pulls’) distribution of the entire sample of GEHRs and HIIGs and the red line shows the best Gaussian fit to the distribution.

In [Figure 2](#) we showcase the $L - \sigma$ relation for the HIIGs and anchor samples. The data encompass four distinct groups, as explained above. The red line in the diagram represents the best linear fit to the data, accounting for uncertainties in both luminosity and velocity dispersion axes. Atop the figure we present the slope and intercept values of this best-fit line, along with their respective uncertainties. Additionally, we quantify the standard deviation of the logarithm of the luminosity ($\log L$) around the best fit, providing a measure of the scatter in the data. The total number of objects in the combined sample is also noted, offering a sense of the statistical robustness of the analysis. The inset in the figure displays the normalised residuals (or ‘pulls’) distribution for the entire dataset. The best Gaussian fit to these residuals is represented by the red line showing that the pulls distribution follows closely the fit. This comprehensive analysis of the $L - \sigma$ relation across a diverse set of GEHRs and HIIGs, including the latest JWST data, provides valuable insights into the underlying physics of these galaxies and contributes significantly to our understanding of galactic dynamics and star formation processes.

[Figure 3](#) depicts the 1σ and 2σ likelihood contours derived from a comprehensive global fit applied to our HIIGs and anchor samples. This fit encompasses all free parameters, both nuisance and cosmological, within the framework of a model featuring an evolving DE EoS parameter. The resultant parameter space constraints, as elucidated in this figure and also from [Table 2](#), demonstrate a high degree of consistency with other recent determinations in the field ([Scolnic et al. 2018](#); [Brout et al. 2022](#)). A comparative analysis of the Figure of Merit (FoM) with that reported in [González-Morán et al. \(2021\)](#) reveals a notable improvement of approximately 6.7% in our results.

Table 2. Marginalised best-fit parameter values and associated 1σ uncertainties for the HIIGs and anchor samples. Values enclosed in parentheses indicate parameters that were held constant during the analysis.

Data Set	α	β	h	Ω_m	w_0	w_a	N
HIIG	—	(5.022 ± 0.058)	—	$0.282^{+0.037}_{-0.045}$	(-1.0)	(0.0)	195
HIIG	—	(5.022 ± 0.058)	—	$0.278^{+0.092}_{-0.051}$	$-1.21^{+0.45}_{-0.40}$	(0.0)	195
HIIG	(33.268 ± 0.083)	(5.022 ± 0.058)	0.715 ± 0.018	$0.267^{+0.038}_{-0.048}$	(-1.0)	(0.0)	195
HIIG	(33.268 ± 0.083)	(5.022 ± 0.058)	0.718 ± 0.020	$0.278^{+0.091}_{-0.050}$	$-1.22^{+0.46}_{-0.40}$	(0.0)	195
Anchor+HIIG	33.276 ± 0.110	4.997 ± 0.089	0.730 ± 0.038	(0.3)	(-1.0)	(0.0)	231
Anchor+HIIG	33.276 ± 0.138	4.997 ± 0.113	0.730 ± 0.040	$0.335^{+0.044}_{-0.055}$	(-1.0)	(0.0)	231
Anchor+HIIG	33.285 ± 0.138	4.989 ± 0.113	0.731 ± 0.039	$0.302^{+0.12}_{-0.069}$	$-1.01^{+0.52}_{-0.29}$	(0.0)	231
Anchor+HIIG	33.290 ± 0.137	4.986 ± 0.112	0.730 ± 0.039	$0.321^{+0.10}_{-0.063}$	$-0.91^{+0.55}_{-0.33}$	$-0.71^{+0.65}_{-1.2}$	231

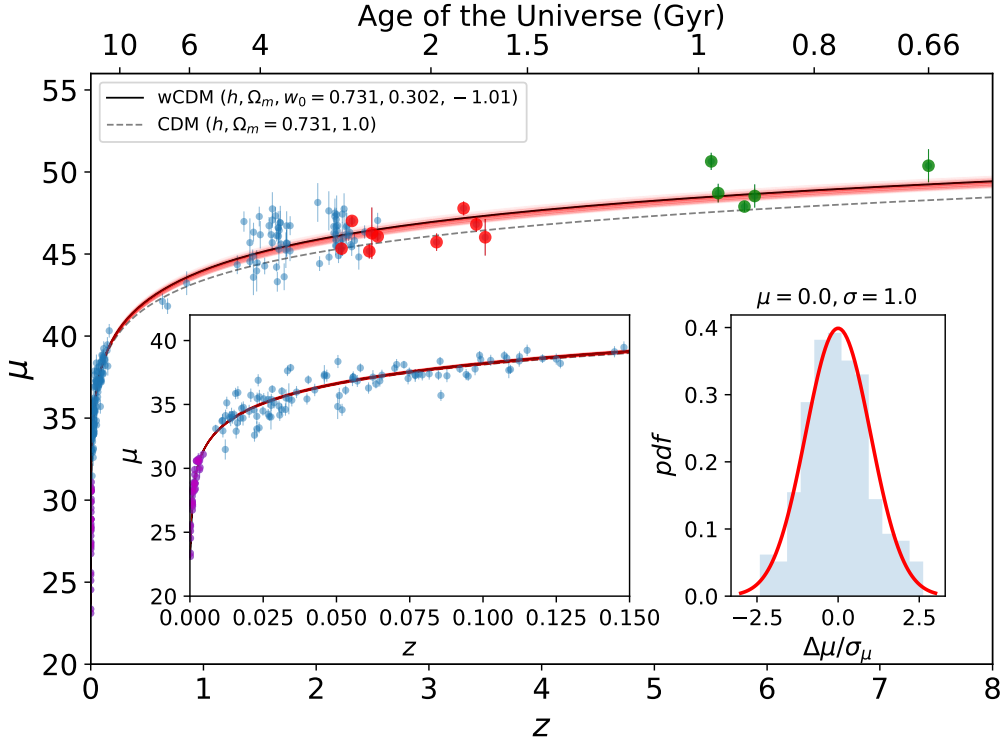


Figure 1. Hubble diagram for the HIIGs and anchor samples. z is the redshift and μ is the distance modulus. In magenta we present the anchor sample of 36 objects which have been analysed in Fernández Arenas et al. (2018); in blue, the full sample of 181 HIIGs which have been analysed in González-Morán et al. (2021); in red we present the 9 new HIIGs from Llerena et al. (2023) and in green the 5 new HIIGs studied with JWST by de Graaff et al. (2024). The inset at the left shows a close-up of the Hubble diagram for $z \leq 0.15$. The black line illustrates the cosmological model that best fits the data with the red shaded area representing the 1σ uncertainties to the model, while the grey dashed line is a flat cosmological model without dark energy. The inset at the right presents the pulls probability density function (pdf) of the entire sample of GEHRs and HIIGs and the red line shows the best Gaussian fit to the pdf.

5 DISCUSSION AND CONCLUSIONS

The observation that the $L-\sigma$ relation remains valid to high-redshifts ($z > 3$) HIIGs, extending to the epoch of reionization, unveils a remarkable uniformity in H II galaxy properties over vast cosmic timescales. This continuity is not just a testament to the robustness of the $L-\sigma$ relation as a cosmological tool but also illuminates the fundamental processes governing formation and evolution of galaxies in the early Universe.

This result has also profound implications for our under-

standing of star formation processes in the early Universe. It suggests that the photo-kinematical properties of massive young clusters, which ionise GEHRs and HIIGs, have remained unchanged for most of the age of the Universe. This conclusion challenges models and assumptions about the non-universality of star formation mechanisms (Bastian et al. 2010; Ziegler et al. 2022).

The constraints on cosmological parameters deduced from our dataset, as delineated in Table 2 and Figure 3, specifically our constraints on the space $\{h, \Omega_m, w_0\} = \{0.731 \pm 0.039, 0.302^{+0.12}_{-0.069}, -1.01^{+0.52}_{-0.29}\}$ (stat) from GHIIR and HIIG

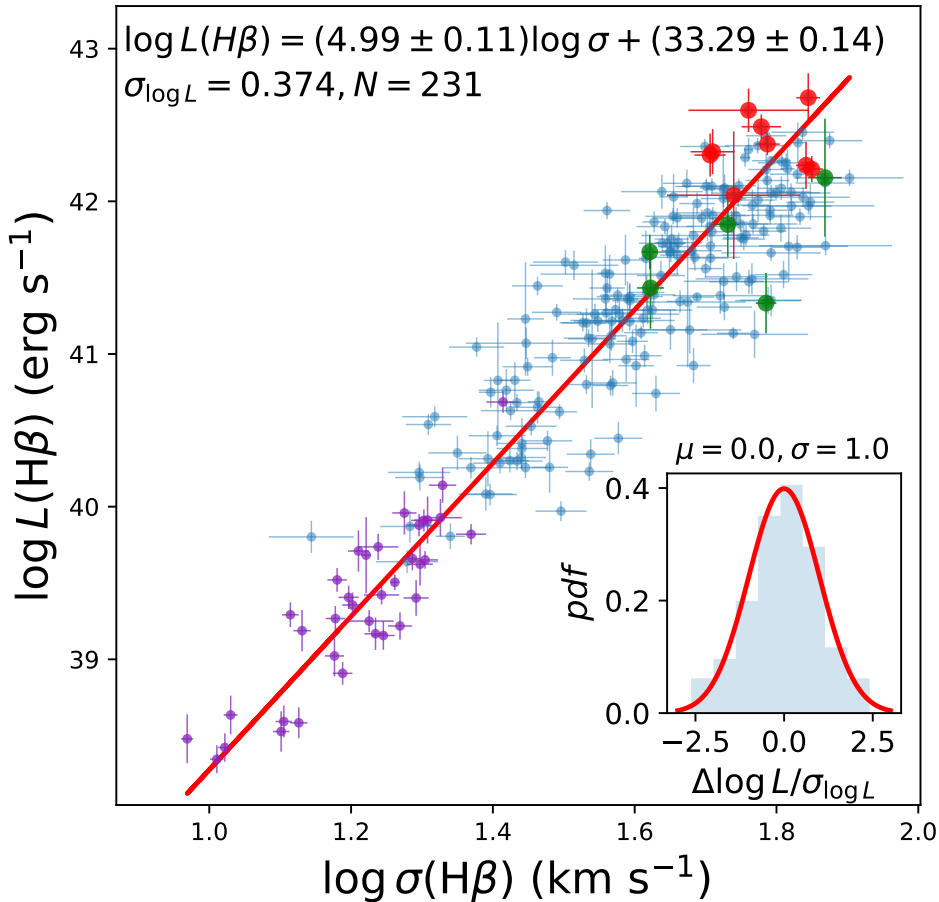


Figure 2. The $L - \sigma$ relation of the HIIGs and anchor samples. The data points follow the same colour code for the different samples as in the previous figure. The red line shows the best linear fit to the data, including the uncertainties in both axis. At the top of the figure we present the values of the slope and intercept of the best fit including their uncertainties. We also show the standard deviation of $\log L$ around the best fit and the total number of objects in the sample. The inset shows the pulls distribution of the entire sample of GEHRs and HIIGs and the red line shows the best Gaussian fit to the distribution.

alone, are closely aligned with the latest results from the Pantheon+ analysis of 1550 SNIa $\{h, \Omega_m, w_0\} = \{0.735 \pm 0.011, 0.334 \pm 0.018, -0.90 \pm 0.14\}$ (Brout et al. 2022). This concordance underscores the robustness and relevance of our findings in the broader context of contemporary cosmological research.

In their study of the $L - \sigma$ relation for HIIGs as cosmological distance indicators, Cao & Ratra (2024) suggest that the relation exhibits a significantly flatter slope for high- z HIIGs compared to their low- z counterparts. This hypothesis carries substantial implications for employing HIIGs in determining cosmological distances. However, the flattening of the $L - \sigma$ slope at high- z reported by Cao & Ratra (2024) is a direct consequence of the very restricted luminosity range accessible due to observational limits, which at high redshift predominantly capture the more luminous galaxies. This limited dynamical range in luminosity leads to a small value of the fitted slope, a concept that is supported by analyses indicating that the $L - \sigma$ slopes for high- z and appropriately matched low-

z samples are statistically indistinguishable when comparing similar luminosity ranges. Additionally, the $L - \sigma$ relation may be affected by systematic variations in age, metallicity, and extinction corrections, necessitating meticulous control over these parameters in cosmological studies. Future research aimed at broadening the $L - \sigma$ application to a more diverse set of galaxy samples, including lensed GHIIRs and HIIGs (see Terlevich et al. (2016) for an example), could further elucidate the relation’s validity across varied cosmic conditions, thereby confirming its universality and enhancing its utility in cosmology.

In our endeavour to refine the independent determination of cosmological parameters using HIIGs, the incorporation of additional data from the JWST up to and above $z \sim 9$ promises to be invaluable. The unparalleled sensitivity and resolution of JWST, capable of probing the early Universe, offer an unprecedented opportunity to observe HIIGs at higher redshifts. This extended observational reach is pivotal, as it allows for the exploration of the Universe’s expansion dynam-

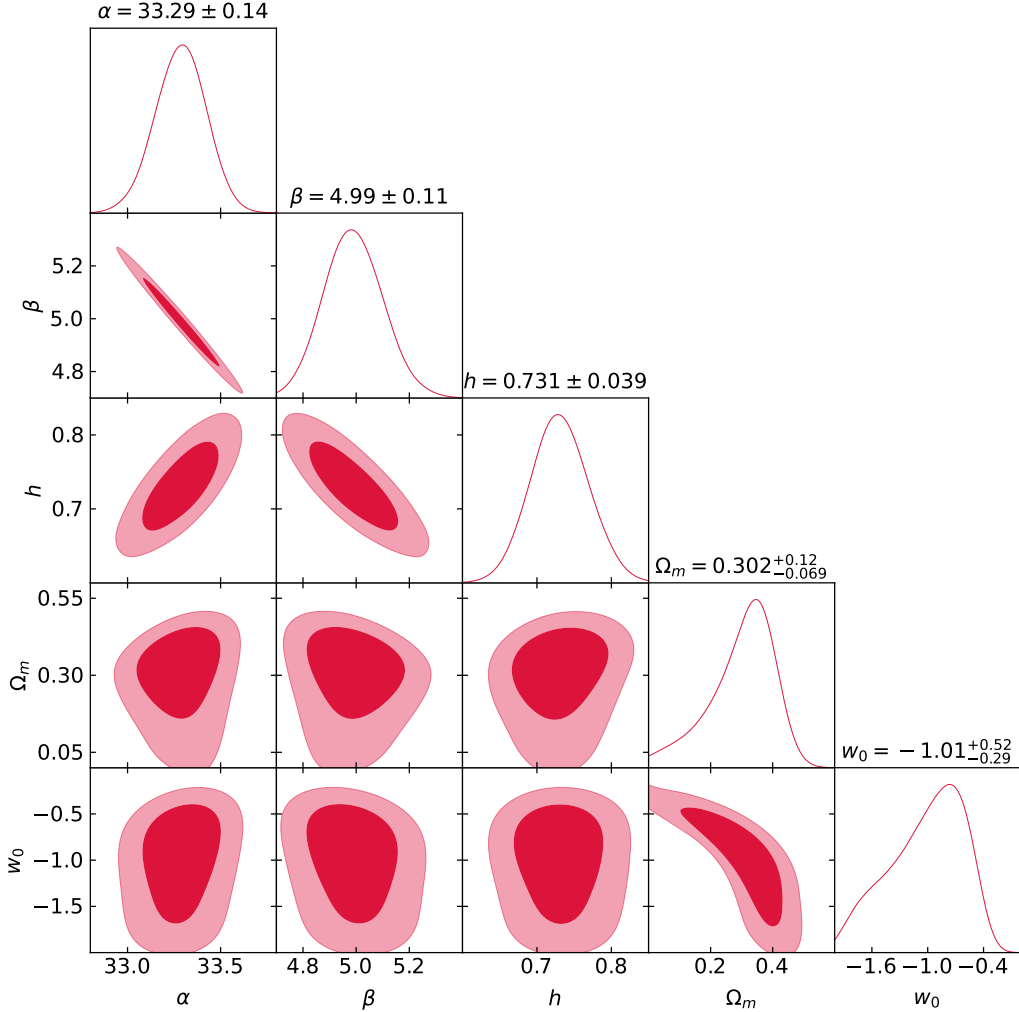


Figure 3. Likelihood contours corresponding to the 1σ and 2σ confidence levels in the $\{\alpha, \beta, h, \Omega_m, w_0\}$ space for the joint HIIGs and anchor samples.

ics under different cosmological conditions, thereby providing a more comprehensive understanding of the evolution of Ω_m , the matter density parameter, and w_0 , the dark energy equation of state parameter.

The observation of distant HIIGs with JWST not only enhances the statistical power of our analysis, but by enormously extending the accessible redshift range allows to test the consistency of the Λ CDM model and the possible evolution of dark energy over a broader span. Moreover, this approach addresses potential biases inherent in current datasets predominantly stemming from their limited redshift range. The use of a single and independent distance indicator over an extremely wide range of cosmic history, with an increased data set is crucial for reducing statistical uncertainties and refining the constraints on $\{h, \Omega_m, w_0\}$.

Further observations from JWST will enable a more detailed examination of the intrinsic properties of HIIGs. This deeper insight is essential for the calibration of the $L - \sigma$ relation and possible mitigation of systematic uncertainties on the derived parameters. By enhancing our understanding of the physical processes governing HIIGs, we can better

interpret their $L - \sigma$ relation, a fundamental factor in the measurement of cosmological parameters.

Our analysis introduces novel insights into the evolution of the Universe. By leveraging this new data, we significantly enhance the existing narrative of cosmic history. Our results add to the understanding of the early Universe conditions and their role in the formation and evolution of galaxies setting the stage for expanding the exploration of the photo-kinematical properties of massive regions of star formation.

DATA AVAILABILITY

The datasets supporting the conclusions of this article, including the data used for generating the figures, are available in the references given at the Data Sets section and from the corresponding author upon reasonable request.

CODE AVAILABILITY

AstroPy [Astropy Collaboration et al. \(2022\)](#), Multinest [Feroz et al. \(2009, 2019\)](#) and PyMultinest [Buchner et al. \(2014\)](#), are all publicly available, while the code used for the data analysis and figure generation for this article is publicly available via GitHub at <https://github.com/blackdragonae/hiigs>

ACKNOWLEDGEMENTS

RCh and DF-A acknowledge support from the CONACYT research grant CF2022-320152. RA acknowledges the support of project PID2023-147386NB-I00 and the Severo Ochoa grant CEX2021-001131-S funded by MCIN/AEI/10.13039/50110001103. ML1 acknowledges support from the PRIN 2022 MUR project 2022CB3PJ3 - First Light And Galaxy aSsembly (FLAGS) funded by the European Union – Next Generation EU.

REFERENCES

- Astropy Collaboration et al., 2022, *ApJ*, **935**, 167
 Baker W. M., et al., 2025, *Nature Astronomy*, **9**, 141
 Bastian N., Covey K. R., Meyer M. R., 2010, *ARA&A*, **48**, 339
 Bergeron J., 1977, *ApJ*, **211**, 62
 Blake C., et al., 2011, *MNRAS*, **418**, 1707
 Bordalo V., Telles E., 2011, *ApJ*, **735**, 52
 Brout D., et al., 2022, *ApJ*, **938**, 110
 Buchner J., et al., 2014, *A&A*, **564**, A125
 Bunker A. J., et al., 2024, *A&A*, **690**, A288
 Cao S., Ratra B., 2024, *Phys. Rev. D*, **109**, 123527
 Chávez R., Terlevich E., Terlevich R., Plionis M., Bresolin F., Basilakos S., Melnick J., 2012, *MNRAS*, **425**, L56
 Chávez R., Terlevich R., Terlevich E., Bresolin F., Melnick J., Plionis M., Basilakos S., 2014, *MNRAS*, **442**, 3565
 Chávez R., Plionis M., Basilakos S., Terlevich R., Terlevich E., Melnick J., Bresolin F., González-Morán A. L., 2016, *MNRAS*, **462**, 2431
 Chevallier M., Polarski D., 2001, *International Journal of Modern Physics D*, **10**, 213
 Dicus D. A., Repko W. W., 2004, *Phys. Rev. D*, **70**, 083527
 Dorner, B. et al., 2016, *A&A*, **592**, A113
 Eisenstein D. J., et al., 2005, *ApJ*, **633**, 560
 Erb D. K., Steidel C. C., Shapley A. E., Pettini M., Reddy N. A., Adelberger K. L., 2006, *ApJ*, **646**, 107
 Fernández Arenas D., et al., 2018, *MNRAS*, **474**, 1250
 Feroz F., Hobson M. P., 2008, *MNRAS*, **384**, 449
 Feroz F., Hobson M. P., Bridges M., 2009, *MNRAS*, **398**, 1601
 Feroz F., Hobson M. P., Cameron E., Pettitt A. N., 2019, *The Open Journal of Astrophysics*, **2**, 10
 Freedman W. L., Madore B. F., Scowcroft V., Burns C., Monson A., Persson S. E., Seibert M., Rigby J., 2012, *ApJ*, **758**, 24
 Gardner J. P., et al., 2006, *Space Sci. Rev.*, **123**, 485
 González-Morán A. L., et al., 2019, *MNRAS*, **487**, 4669
 González-Morán A. L., et al., 2021, *MNRAS*, **505**, 1441
 Gordon K. D., Clayton G. C., Misselt K. A., Landolt A. U., Wolf M. J., 2003, *ApJ*, **594**, 279
 Jaffe A. H., et al., 2001, *Physical Review Letters*, **86**, 3475
 Kunth D., Östlin G., 2000, *A&ARv*, **10**, 1
 Linder E. V., 2003, *Physical Review Letters*, **90**, 091301
 Llerena M., et al., 2023, *A&A*, **676**, A53
 Maseda M. V., et al., 2014, *ApJ*, **791**, 17
 Masters D., et al., 2014, *ApJ*, **785**, 153
 Melnick J., Terlevich R., Moles M., 1988, *Monthly Notices of the Royal Astronomical Society*, **235**, 297
 Nesseris S., Perivolaropoulos L., 2005, *Phys. Rev. D*, **72**, 123519
 Peebles P. J. E., Ratra B., 1988, *ApJ*, **325**, L17
 Peebles P. J., Ratra B., 2003, *Reviews of Modern Physics*, **75**, 559
 Perlmutter S., et al., 1999, *ApJ*, **517**, 565
 Planck Collaboration et al., 2014, *A&A*, **571**, A16
 Planck Collaboration et al., 2016, *A&A*, **594**, A13
 Plionis M., Terlevich R., Basilakos S., Bresolin F., Terlevich E., Melnick J., Chavez R., 2011, *MNRAS*, **416**, 2981
 Pryke C., Halverson N. W., Leitch E. M., Kovac J., Carlstrom J. E., Holzzapfel W. L., Dragovan M., 2002, *ApJ*, **568**, 46
 Ratra B., Peebles P. J. E., 1988, *Phys. Rev. D*, **37**, 3406
 Riess A. G., et al., 1998, *The Astronomical Journal*, **116**, 1009
 Riess A. G., et al., 2016, *ApJ*, **826**, 56
 Riess A. G., et al., 2018, *ApJ*, **855**, 136
 Scolnic D. M., et al., 2018, *ApJ*, **859**, 101
 Searle L., Sargent W. L. W., 1972, *ApJ*, **173**, 25
 Spergel D. N., et al., 2007, *ApJS*, **170**, 377
 Terlevich R., Melnick J., 1981, *MNRAS*, **195**, 839
 Terlevich R., Terlevich E., Melnick J., Chávez R., Plionis M., Bresolin F., Basilakos S., 2015, *MNRAS*, **451**, 3001
 Terlevich R., et al., 2016, *A&A*, **592**, L7
 Wang Y., 2008, *Phys. Rev. D*, **77**, 123525
 Wang Y., Mukherjee P., 2006, *ApJ*, **650**, 1
 Wetterich C., 1988, *Nuclear Physics B*, **302**, 668
 Ziegler J. J., Edwards T. D. P., Suliga A. M., Tamborra I., Horiuchi S., Ando S., Freese K., 2022, *MNRAS*, **517**, 2471
 de Graaff A., et al., 2024, *A&A*, **684**, A87